Compact on-chip dual-band bandpass filter with wide out-of-band suppression based on hybrid coupling technique

Yanzhu Qi, Yazi Cao [*], Bo Yuan, Shichang Chen, Kanglong Zhang, Gaofeng Wang [**]

MOE Engineering Research Center of Smart Microsensors and Microsystems, the School of Electronics and Information, Hangzhou Dianzi University, Hangzhou, Zhejiang, 310018, China

ARTICLE INFO

ABSTRACT

A compact dual-band bandpass filter (BPF) with wide out-of-band suppression based on a hybrid coupling technique is proposed. This BPF consists of two hybrid spiral coupled resonators, in which the electrical coupling and magnetic coupling between resonators can generate two transmission paths for dual bands. This dual-band BPF has wide out-of-band suppression. Moreover, its passband frequency and bandwidth can be readily controlled. To illustrate its working principle, an equivalent circuit with even- and odd-mode analysis is presented. This dual-band BPF is fabricated using a silicon integrated passive device (IPD) technology. The fabricated dual-band BPF has a compact size of 1.6 mm × 0.54 mm × 0.23 mm and is measured. The measured results show that this dual-band BPF can generate two bands at 2.45 GHz and 6.15 GHz. In addition, more than 20 dB of suppression is achieved from 7.8 to 20 GHz ($8.16f_0$). The simulated and measured results exhibit good agreements.

1. Introduction

With development of wireless communication systems, dual-band BPFs are widely used in wireless communication systems to provide capability of multiple operating bands and reduce the size of the RF front end. Dual-band BPFs with high performance, such as low loss, compact size, and large power capacity have been reported in many works with various design methods and configurations [1–15].

Dual-band BPFs using cavity structures, such as rectangular and circular waveguides [1,2], can achieve low loss and high-power performance, but the size is relatively large. To reduce the size, the cavity filter has adopted multimode design [2] or dielectric resonator [3]. Moreover, printed circuit board (PCB) can achieve multi-layer structures and have a much smaller size than cavities, and thus many dual-band BPFs were designed using multi-layer planar structures such as microstrips [4], substrate integrated waveguide [5,6] and substrate integrated suspended line [7]. There are two main approaches to improve out-of-band suppression of dual-band BPFs. One is to improve out-of-band suppression by introducing transmission zeros [8,9], and the other is to achieve a wider stopband [10–12].

Dual-band BPFs based on the PCB process achieve tradeoffs in size

and performance. To further reduce the size, many dual-band BPF designs have used the low-temperature cofired ceramic (LTCC) process [13,14]. These works reported compact dual-band BPFs with various degrees of performance and size reduction. In addition, the small size of mobile devices makes system in package (SiP) an inevitable trend. The design based on the integrated passive device process is much more compact and thinner compared to LTCC, and thus more favorable for integration in SiP [15]. As a consequence, the IPD technology becomes the most popular in recent years [16,17].

In this letter, a compact dual-band BPF with wide out-of-band suppression based on a hybrid coupling technique is presented. This BPF consists of two hybrid spiral coupled resonators, in which the electrical coupling and magnetic coupling between resonators can generate two transmission paths for dual bands. Meanwhile the passband frequency and bandwidth can be readily controlled, and the proposed filter can achieve wide out-of-band suppression. The filter has a compact structure. To illustrate the working principle, an equivalent circuit with even- and odd-mode analysis is discussed. The proposed dual-band BPF is fabricated using a silicon IPD process. The fabricated dual-band BPF shows a competitive performance compared with the state-of-the-art works.

---

* Corresponding author.
** Corresponding author.
    E-mail addresses: caoyazi@hdu.edu.cn (Y. Cao), gaofeng@hdu.edu.cn (G. Wang).

Table 1
Comparison of the proposed BPF with other recent works.

Ref.	f_0/f_1 (GHz)	Rej (dB)/Stopband	IL (dB)	FBW (%)	Size (λ_g^2)	Tech
[10]	8/11.4	20/2.34 f_0	2.26/3.07	3.01/2.46	1.66 × 1.31	PCB
[11]	2.44/3.5	20/2.23 f_0	2.07/2.21	4.98/2.7	0.45 × 0.19	PCB
[13]	3.32/5.17	–	1.38/1.53	25.5/14.2	0.31 × 0.16$^+$	LTCC
[16]	35/70	–	3/3.3	32.9/22.4	0.31 × 0.14$^+$	CMOS
[17]	28/50	–	0.58/3.29	39.5/5	–	GaAs
This work	2.45/6.17	20/8.16 f_0	2.78/3.65	28.6/15.2	0.048 × 0.0162	HRS
		25/7.96 f_0				

FBW: Fractional Bandwidth, 3 dB bandwidth; λ_g: The guide wavelength at f_0; HRS: High Resistivity Silicon. $^+$: Calculate from the data given.

(a)

(b)

(c)
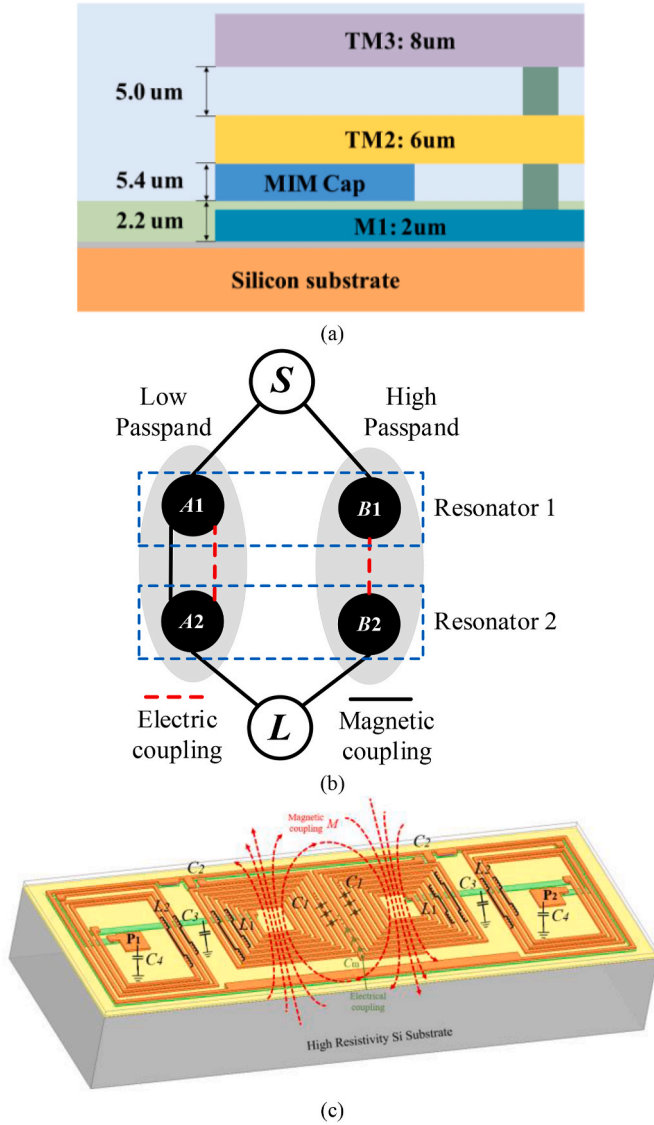
Fig. 1. Proposed dual-band IPD bandpass filter. (a) Stack-up of the applied silicon based IPD technology. (b) Circuit topology. (c) 3D view of layout.

(a)

(b)

(c)

Fig. 2. Schematic of the proposed dual-band BPF. (a) Overall equivalent circuits model. (b) Even-mode equivalent circuit model. (c) Odd-mode equivalent circuit model.

2. Design and analysis

2.1. Structure of dual-band BPF

A silicon IPD process is herein used for fabrication of the proposed dual-band BPF. Fig. 1(a) shows stack-up of the silicon IPD process, in which metal layer M1 is of aluminum and thick metal layers TM1 and TM2 are of copper. The additional metal-insulator-metal (MIM) layer is placed between M1 and TM2. In addition, the height of the silicon substrate is 250 μm. The relative dielectric constant of silicon substrate is 11.7, and the dielectric loss tangent is 0.003.

The circuit topology of the proposed dual-band BPF is shown in Fig. 1 (b), in which the filtering response of lower passband mainly depends on the filtering channel A, while the higher passband is realized by the filtering channel B. Each channel has two resonators, and there is an electromagnetic (EM) coupling between the two resonators.

The layout of the proposed dual-band BPF is shown in Fig. 1(c). The main structure consists of two spiral resonators placed symmetrically. C_1 and L_1 denote the self-capacitance and self-inductance of the spiral resonator, respectively. C_2 represents the capacitive coupling between the end of the spiral resonator and the ground. C_3 represents the bypass
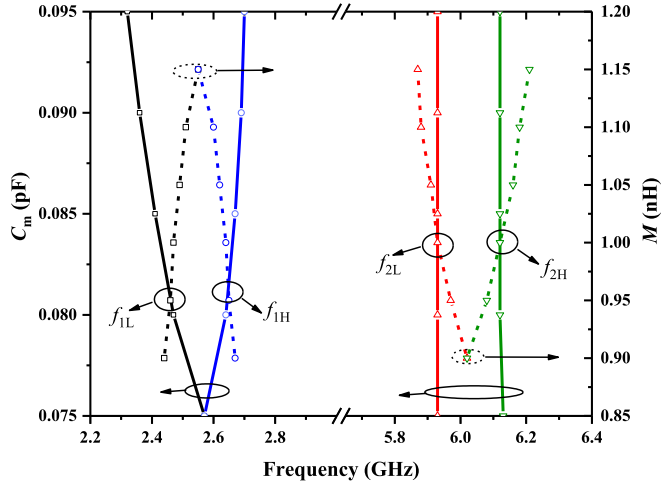
Fig. 3. Circuit simulated TPs frequency, while C_m is swept from 0.075 to 0.095 pF and M is swept from 0.85 to 1.2 pF, $L_1 = 7$ nH, $L_2 = 8$ nH, $C_1 = 0.09$ pF, $C_2 = 0.15$ pF, $C_3 = 0.1$ pF and $C_4 = 0.1$ pF.

capacitance between the middle line and the ground. L_2 denote the inductance of the high-frequency resonant path. C_4 represents the bypass capacitance between the pad and the ground. The loaded capacitor C_2 can be used to control the resonant frequency without adding much extra area since the physical size of the capacitor is much smaller than that of the inductor.

2.2. Analysis of dual-band BPF

To illustrate the working principle, an equivalent circuit model is given in Fig. 2(a). The even- and odd-mode analysis method is applied here due to the symmetrical topology. Fig. 2(b) and (c) show the even- and odd-mode circuits, respectively. The admittances of the even- and odd-mode circuits are denoted as Y_{ine} and Y_{ino}, respectively, which can be obtained as follows:

$$Y_{ine} = \left[\left(\frac{1}{j\omega(L_1 + M)} + j\omega C_1 \right) // j\omega C_2 + j\omega C_3 \right] // \frac{1}{j\omega L_2} + j\omega C_4 \quad (1)$$

$$Y_{ino} = \left[\left(\frac{1}{j\omega(L_1 - M)} + j\omega C_1 \right) // j\omega(C_2 + 2C_m) + j\omega C_3 \right] // \frac{1}{j\omega L_2} + j\omega C_4 \quad (2)$$

Then the scattering parameters of the two-port network can be expressed as [17]:

$$S_{11} = \frac{Y_0^2 - Y_{ine} Y_{ino}}{(Y_0 + Y_{ine})(Y_0 + Y_{ino})} \quad (3)$$

$$S_{21} = \frac{Y_0(Y_{ine} - Y_{ino})}{(Y_0 + Y_{ine})(Y_0 + Y_{ino})} \quad (4)$$

where Y_o is the load admittance. For the proposed resonator with two ports, it is possible to find the transmission pole (TP) by solving $S_{11} = 0$. Considering the coupling between two resonators, the mixed coupling coefficient k_X between every two adjacent resonators can be represented by Ref. [18]:

$$k_X \approx k_e + k_m = \frac{C_m}{C_2} + \frac{M}{L_1} \quad (5)$$

where M and C_m denote the magnetic and electrical couplings, respectively. By tuning the values of M and C_m, the bandwidth of the dual-band BPF, which is related to the coupling coefficient, can be adjusted.

To understand the effects of electrical and magnetic couplings on the TPs distribution, Fig. 3 shows how the frequency response of TPs varies
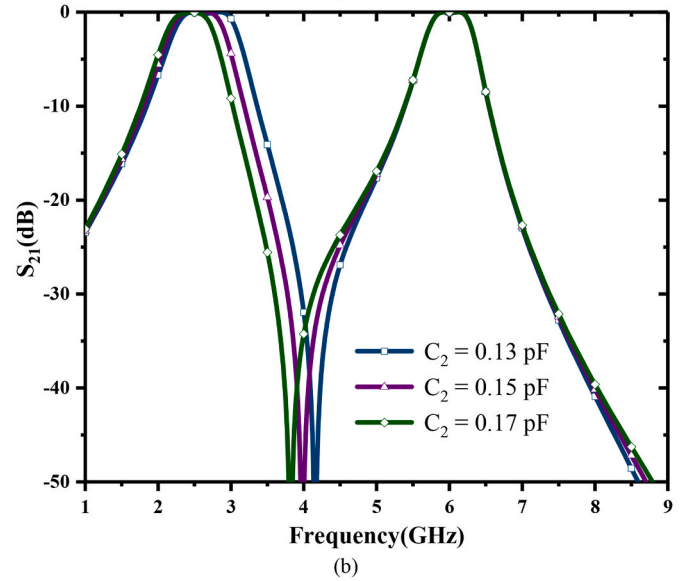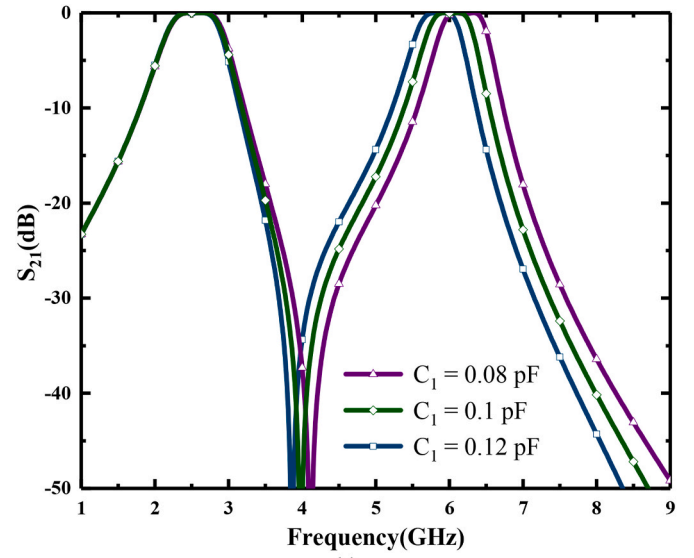

(a)

(b)

Fig. 4. Circuit simulated S_{21} of the dual-band BPF. (a) C_1 is swept from 0.08 to 0.12 pF. (b) C_2 is swept from 0.13 to 0.17 pF ($L_1 = 7$ nH, $L_2 = 8$ nH, $L_3 = 1$ nH, $C_m = 0.08$ pF, $C_3 = 0.1$ pF and $C_4 = 0.1$ pF)

with different values of C_m and M. With increasing C_m, the coupling is strengthened and the distance between the two poles in the low-frequency passband increase. On the other hand, the two poles in the high-frequency passband are unchanged. It indicates that the high-frequency passband is not controlled by the electrical coupling. With increasing M, the coupling is strengthened and the distance between the two poles in the low-frequency passband decreases and the bandwidth narrows. On the other hand, the distance between the two poles of the high-frequency passband increases. It indicates that the magnetic coupling can control the two passbands and have opposite effects on the two passbands. Therefore, carefully adjusting the values of C_m and M can adjust the bandwidth of the high and low frequency passbands, respectively.

The two passband frequencies can be controlled by C_1 and C_2 respectively. As shown in Fig. 4(a), with the increase of capacitor C_1, the high-frequency band moves to the lower frequency, whereas the low-frequency band is virtually unchanged. As shown in Fig. 4(b), with the increase of capacitor C_2, the low-frequency band moves to the lower frequency, whereas the high-frequency band is virtually unchanged. The
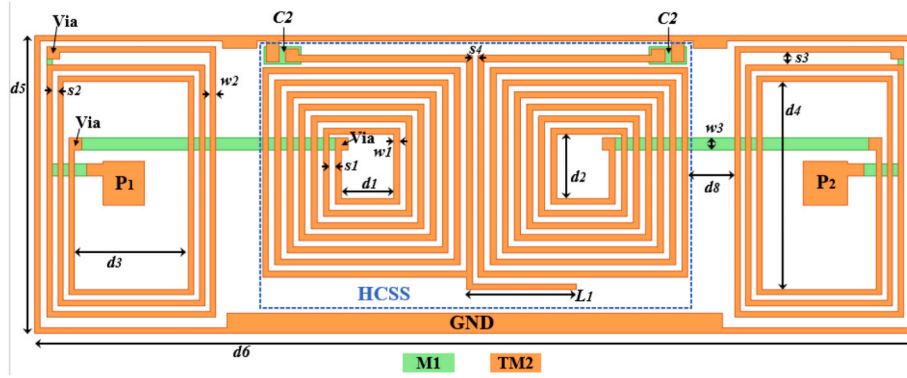
Fig. 5. 2-D layout of the dual-band BPF layout. (Dimensions: $w1 = 11$, $w2 = 10$, $w3 = 23$, $s1 = 11$, $s2 = 10$, $s3 = 23$, $s4 = 10$, $L1 = 200$, $d1 = 95$, $d2 = 116$, $d3 = 207$, $d4 = 377$, $d5 = 540$, $d6 = 1600$, $d7 = 85$. Unit: μm).
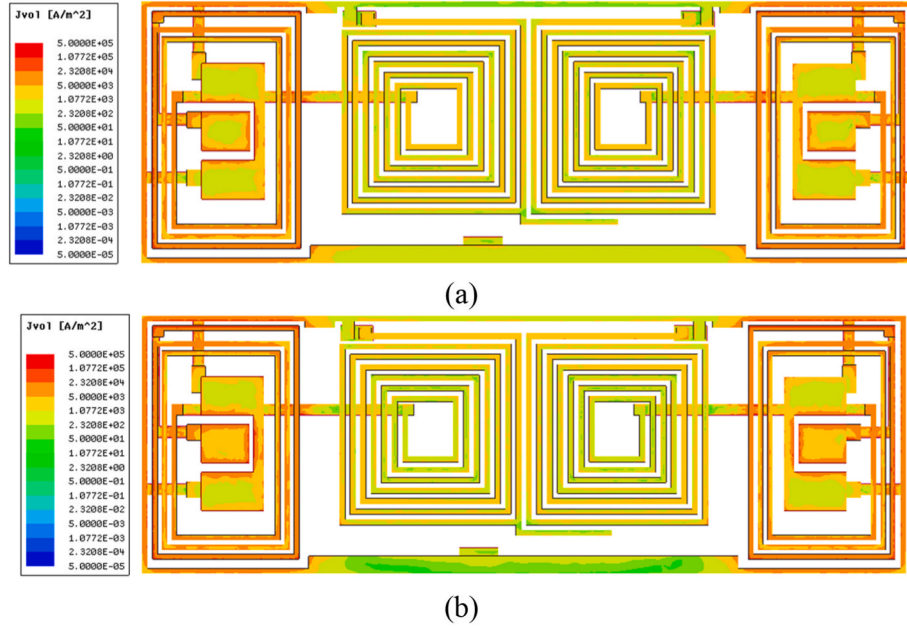

Fig. 6. Current distribution at (a) 12.5 GHz. (b) 17.5 GHz.
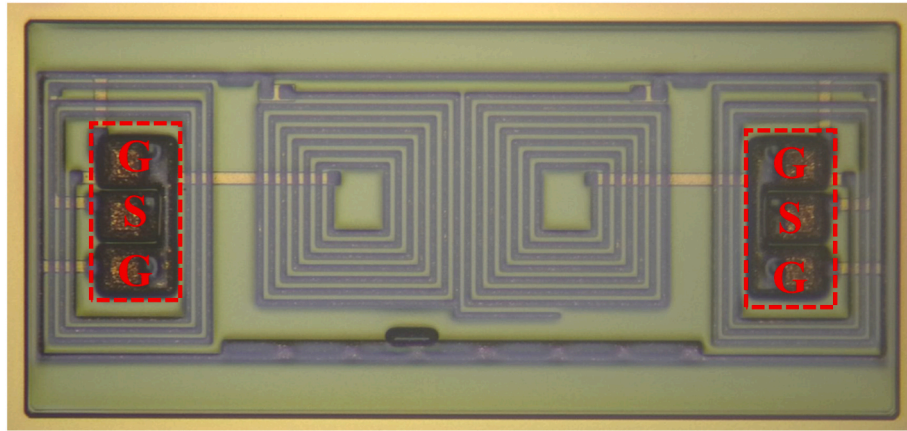

Fig. 7. Die photograph of the proposed dual-band filter.

2-D layout and key dimensions of the proposed dual-band BPF are shown in Fig. 5. It should be noted that due to the limitation of the minimum line width of the process, it is difficult to achieve the capacitance value required by C_m even if the distance s4 between the two spiral coupled resonators adopts the minimum value. Therefore, adding an extra trace of length $L1$ to provide additional capacitance,
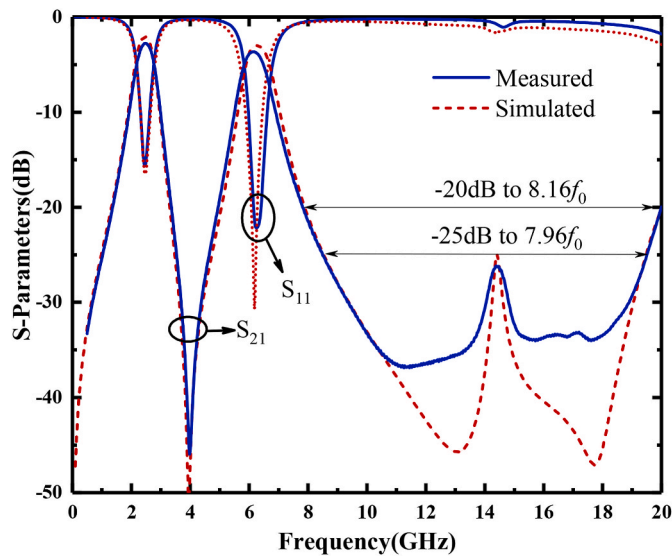
Fig. 8. Comparisons between the EM-simulated and measured results.

adjusting the value of $L1$ can adjust the size of C_m, which plays a role in the layout optimization.

As shown in Fig. 2(a), C_3, C_4 and L_2 in the circuit form a π-type low pass filter circuit, which can improve the out-of-band suppression of the dual passband filter in the high frequency band. The current distribution of the dual-band filter is shown in Fig. 6. At the frequencies of 12.5 GHz and 17.5 GHz, the current is mainly distributed in the spiral structure composed of C_3, C_4 and L_2. Due to its low-pass filtering characteristics, its out-of-band suppression characteristics at 10 GHz–20GHz are improved.

3. Fabrication and measurement

The proposed silicon IPD dual-band BPF design is fabricated and measured to evaluate its performance. The proposed dual-band BPF includes two ground-signal-ground (G-S-G) feeding structures. Fig. 7 shows the final layout of the fabricated dual-band BPF chip with a size of 1.6 mm × 0.54 mm, i.e., 0.0a48 λ_0 × 0.0162 λ_0. This BPF is simulated by UltraEM [19] and is measured by on-wafer probing using the Keysight N5247A vector network analyzer. The results of EM simulation and measurement are compared in Fig. 8. Good agreement between simulated and measured results is clearly observed. Specifically, for the lower passband, the measured center frequency is 2.45 GHz, and the 3-dB bandwidth is from 2.1 GHz to 2.8 GHz (FBW is 28.6 %) with the insertion loss of 2.78 dB. For the upper passband, the center frequency is 6.15 GHz, and the 3-dB bandwidth is from 5.7 GHz to 6.64 GHz (FBW is 15.2 %) with the insertion loss of 3.65 dB. In order to achieve a narrower bandwidth of the two passbands, the two poles in the passbands are merged into one pole by adjusting the coupling. The simulation results show that the proposed filter can achieve a good the insertion loss, but due to the manufacturing tolerance and the loss tangent parameters in the actual processing, the measured insertion loss performance deterioratesFor the stopband, the stopband ranges from 7.82 GHz to 20 GHz ($8.16f_0$) with a suppression of >20 dB, and from 8.5 GHz to 19.5 GHz ($7.96f_0$) with a suppression of >25 dB. Compared to the previous designs, as shown in Table 1, it can be observed that the proposed dual-band BPF has more compact size, high selectivity rejection and wide stopband compared with other designs.

4. Conclusion

In this letter, a miniaturized dual-band BPF based on hybrid coupling technique has been proposed. Using the theoretical analysis of hybrid coupling technique, combined with circuit and electromagnetic simulations, its passband frequency and bandwidth can be easily controlled. The proposed filter achieves the out-of-band rejection of better than 20 dB up to 8.16 times the center frequency. Furthermore, the fabricated dual-band BPF has a compact size of 1.6 mm × 0.54 mm × 0.23 mm. The proposed BPF with the compact size and wide stopband rejection is a promising candidate for the potential applications of Wi-Fi 6 communication systems.

Author statement

Please find submitted the revised version of ID MEJ-D-24-00590, entitled "Compact On-Chip Dual-Band Bandpass Filter with Wide Out-of-Band Suppression Based on Hybrid Coupling Technique", co-authored by Y. Qi, B. Yuan, S. Chen, G. Wang, and me. Here is our Author Statement to agree and publish our paper to MEJ.

Declaration of competing interest

The authors declare that they have no known competing financial interests or personal relationships that could have appeared to influence the work reported in this paper.

Finally, we would like to thank both you and the reviewers for spending time and efforts on this reviewing process.

Data availability

No data was used for the research described in the article.

Acknowledgements

References

[1] D.-S. La, M.-Y. Wang, T.-X. Jiang, C.-X. Zhang, J.-W. Guo, High selectivity cylindrical cavity dual-band bandpass filter with stepped cylinders, IEEE Transactions on Circuits and Systems II: Express Briefs 69 (9) (Sept. 2022) 3759–3763.

[2] Z. Xu, Y. Wu, Q. Dong, W. Wang, Miniaturized dual-band filter using dual-mode dielectric waveguide resonator, IEEE Microw. Wireless Compon. Lett. 32 (12) (Dec. 2022) 1411–1414.

[3] Z. Tan, Q.-Y. Lu, J.-X. Chen, Differential dual-band filter using ground bar-loaded dielectric strip resonators, IEEE Microw. Wireless Compon. Lett. 30 (2) (Feb. 2020) 148–151.

[4] W. Chen, Y. Wu, W. Wang, K. Xu, J. Shi, Synthesis design on wideband single-ended and differential dual-band filtering impedance transformer, IEEE Transactions on Circuits and Systems II: Express Briefs 68 (3) (March 2021) 913–917.

[5] Chenhui Fan, Xiaoxian Liu, Nuo Liu, Yintang Yang, Zhangming Zhu, An effective method to suppress high-order modes of SIW filters with compact size, Microelectron. J. 127 (2022) 105519.

[6] Yi Le, Hongcheng Dong, Guodong Su, Jinsong Zhan, Quan Xing, Jun Liu, A miniaturized and low-loss Q-band SIW bandpass filter based on evanescent-mode in wafer-level packaging process, Microelectron. J. 149 (2024) 106209.

[7] X.-F. Li, J.-K. Xiao, Dual-band bandpass filter based on suspended coplanar waveguide-microstrip hybrid, IEEE Transactions on Circuits and Systems I: Regular Papers 70 (10) (Oct. 2023) 3920–3929.

[8] E. Shankar, K.V.P. Kumar, V.K. Velidi, Design of high selectivity compact dual-band bandpass filter with seven transmission-zeros for GPS and WiMAX applications, IEEE Transactions on Circuits and Systems II: Express Briefs 70 (7) (July 2023) 2395–2399.

[9] H. Chang, W. Sheng, J. Cui, J. Lu, Multilayer dual-band bandpass filter with multiple transmission zeros using discriminating coupling, IEEE Microw. Wireless Compon. Lett. 30 (7) (July 2020) 645–648.

[10] H.-W. Xie, K. Zhou, C.-X. Zhou, W. Wu, Compact SIW diplexers and dual-band bandpass filter with wide-stopband performances, IEEE Transactions on Circuits and Systems II: Express Briefs 67 (12) (Dec. 2020) 2933–2937.

[11] F. Wei, J.H. Yu, C.Y. Zhang, C. Zeng, X.W. Shi, Compact balanced dual-band BPFs based on short and open stub loaded resonators with wide common-mode suppression, IEEE Transactions on Circuits and Systems II: Express Briefs 67 (12) (Dec. 2020) 3043–3047.

[12] J. Tang, H. Liu, Y. Yang, Compact wide-stopband dual-band balanced filter using an electromagnetically coupled SIR pair with controllable transmission zeros and bandwidths, IEEE Transactions on Circuits and Systems II: Express Briefs 67 (11) (Nov. 2020) 2357–2361.

[13] L. Hao, Y. Wu, W. Wang, Y. Yang, Design of on-chip dual-band bandpass filter using lumped elements in LTCC technology, IEEE Transactions on Circuits and Systems II: Express Briefs 69 (3) (March 2022) 959–963.

[14] A. Pourzadi, A. Isapour, A. Kouki, Design of compact dual-band LTCC second-order Chebyshev bandpass filters using a direct synthesis approach, IEEE Trans. Microw. Theor. Tech. 67 (4) (2019) 1441–1451.

[15] Ji-Hu Li, Cong Wang, Luqman Ali, Xiao Tan, Wei Yu-Chen, Ho-Kun Sung, Zhi-Qiang Gao, Shan-Shan Xu, Yang Li, Design and optimization of GaAs-based thin film integrated passive device bandpass filters for 5G communications, Microelectron. J. 139 (2023) 105913.

[16] V.N. Rao Vanukuru, V. Krishna Velidi, CMOS 35/70 GHz dual-band bandpass filter with five transmission zeros using compact stub-loaded coupled-line unit. 2019 IEEE MTT-S International Microwave and RF Conference (IMARC), 2019, pp. 1–3. Mumbai, India.

[17] G. Shen, W. Feng, W. Che, Y. Shi, Y. Shen, Millimeter-wave dual-band bandpass filter with large bandwidth ratio using GaAs-based integrated passive device technology, IEEE Electron. Device Lett. 42 (4) (April 2021) 493–496.

[18] J.-S. Hong, M.J. Lancaster, Microstrip Filters for RF/microwave Applications, John Wiley & Sons, New York, 2001.

[19] UltraEM V202109, Faraday Dynamics, Inc., Hangzhou, Zhejiang, China, 2022.